Chapter 1

Introduction

In .July 1967, Anthony Hewish and Jocelyn Bell while working on a project on inter-planetary scintillation, observed strong periodic signals consistently over a few days. It was possible to rule out interference as it appeared to come from a specific direction in the sky repeatedly. Within a few months it became clear that the signal had an astrophysical origin. The discovery was finally published in February 1968 (Hewisli et al. 1968). The pulsating source was soon identified as a rotating neutron star. This first pulsar, designated PSR B1919+21, had a period of 1.337 seconds. The Nobel prize for the discovery of neutron stars was given to Anthony Hewish in 1974.

About thirty years before the discovery, Baade and Zwicky (1934) proposed neutron stars as end products of stellar evolution. A massive star ($\geq 8M_{\odot}$) after burning its nuclear fuel explodes violently in a spectacular event called 'supernova.' and what is left, behind at, the center is a neutron star. The other way by which neutron stars can be formed are in binaries, where a white dwarf might be accreting mass from its companion and firiallv collapses to form a neutron star. Neutron stars are extremely dense objects with very high magnetic field. It is supported against gravity by the nuclear forces acting between neutrons at high density, as well as the fermi degenerate pressure of the neutrons. They have masses $\sim 1.4M_{\odot}$and are primarily seen as rotation-powered pulsars or accreting X-ray binaries, some of which are accretion-powered pulsars. Rotation-powered pulsars are seen mainly in the radio frequency, while X-ray binaries, as their names suggest, are mainly seen in X-rays. A small number of the rotation-powered pulsars (e.g. the Crab pulsar) have also been seen at high energies (optical. X-rays and γ rays). Work reported in this thesis relates to rotation-powered pulsars only.

1.1 Pulsar-Neutron star Connection

Periodic phenomena observed in astrophysical sources are associated with either rotation or oscillation (vibration). The radio pulses observed by Jocelyn Bell. have a period of 1.33 sec. In 1966, just before the discoverv of pulsars, Melzer & Thorne showed that a white dwarf can have radial oscillations of periods about 10 sec. For oscillations driven by pure gravity the period is proportional to $(G\rho)^{-1/2}$ where ρ is the density of the system. For white dwarfs with average density of 10^7gcm^{-3} the oscillation period is in the range of 10 sec and that for neutron stars with average density 10^{14}gcm^{-3} about 5 msec. For white dwarfs, the period can reduce to a minimum of 1 sec if elasticity is invoked as the restoring force. For neutron stars radial oscillations cannot explain the 1.33 sec periodicity observed, the expected oscillation timescales being in the range of milliseconds. Soon, following the discovery of rather short-period pulsars like Vela (89 rnsec) and Crab (33 msec), the theorv of pulsars as oscillating white-dwarfs failed. To identify objects and a suitable mechanism which can explain the observed periods a theory was conclusively put forward by Gold (1968) and Pacini (1968). The theory predicted that pulsars are rotating neutron stars. This conclusion was reached following a simple estimate of balancing the centrifugal force and the gravitational force in a. rotating star. A star of uniform density ρ will break apart due to centrifugal force if its spin period is shorter than

$$P_{\text{min}} = (3\pi/G\rho)^{1/2}. \tag{1.1}$$

The observed period of 1.33 sec of PSR B1919+21 would be the limiting spin period of a star of density $\sim 10^8$gcm^{-3}, which is the density range for white dwarfs, but for the shorter periods of Crab and Vela pulsars the required density would be well above that of white-dwarfs. For neutron stars, on the other hand, the fastest possible spin is $P_{\text{min}} \sim 1$ msec. The limit on the spin thus provides a stringent condition for source identification. The naturally favoured model which can explain the observed periods of pulsars, is a rotating neutron star. The 'millisecond pulsar', PSR B1937+21 with period of 1.55 msec is the best example of a fast rotating neutron star.

To explain the clock-like pulses from rotating neutron stars the idea of a 'lighthouse' effect is invoked. It is believed that there are two emission beams separated by 180° on the spherical surface of the neutron star. As the star rotates, the emission beam crosses the line-of-sight of an earth-bound observer and a pulse of emission is observed. The observed radio pulses require the radio source to be compact, localised and directional. The emission region is thought to be located on the open field lines of the magnetic dipole associated with the star (refer Fig. 1.1). It is observed that the period of the pulsar slows down at a steadv rate with tirne. For example in the Crab Pulsar the slow down rate as observed by Richards and Comella (1969) mas 36.48 ±0.04 nanosec per dav. The slowdown can be understood in terms of the energy carried awav by magnetic dipole radiation and/or charged particle stream from the pulsar at the cost of the rotational energy of the star (Pacini 1968, Goldreich & Julian 1969). Note that mechanisms involving stellar oscillations cannot explain the observed slow down in pulsars.

1.2 Pulsar Parameters

The most fundamental parameter of a pulsar is of course the **period (P)** of the pulsar. Today more than 1000 pulsars are known. The period ranges from 1.5 msec to 8.5 sec. Pulsars with periods less than 20 msec arc usually referred to as 'millisecond pulsars' and those with longer periods as 'normal pulsars' (refer Fig.1.2). Even before the discoverv of pulsars, Pacini (1967) suggested that the Crab Nebula (which is the remnant of a Supernova observed bv the Chinese Astronomers in 1054 A.D.) is powered by the magnetic dipole radiation from a rapidly rotating highly magnetized neutron star. The amount of energy lost by dipole radiation comes at the expense of the rotational energy of the neutron star, and the energy balance equation is given by,

$$-\frac{d}{dt}(I\omega^2/2) = \frac{2}{3c^3}|\mathbf{m}|^2 w^4 sin^2\alpha \tag{1.2}$$

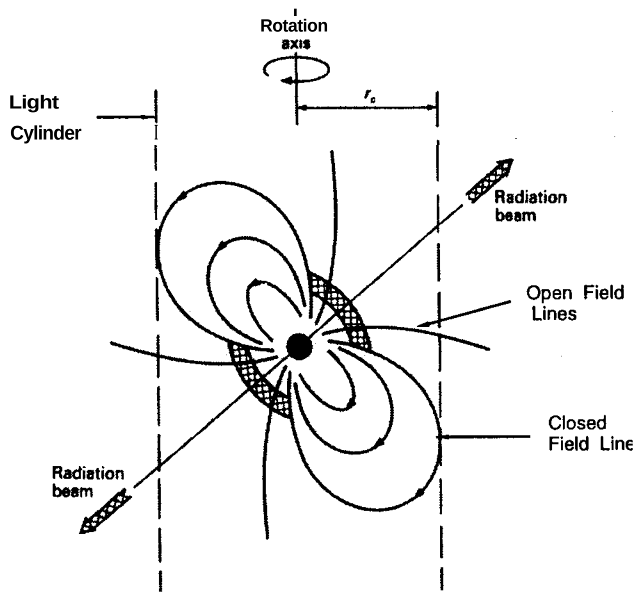

Figure 1.1: Schematic representation of a pulsar magnetosphere (Figure adopted from Lyne & Smith, 1998). The dashed line which is at a distance r_c from the rotation axis, defines the light cylinder radius. The closed field lines are the dipolar magnetic field lines which close within the light cylinder, while the open field lines does not, as shown in the figure. Radio emission region is represented by the cross-hatched region.

where **I** is the moment of inertia of the neutron star, w $= 2\pi/P$ is the angular velocity, a is the angle between the dipole magnetic axis and the rotation axis and m is the dipole magnetic moment. This loss of energy is the cause for slow down of pulsars as observed. The rate of change of angular velocity follows from equation (1.2) as,

$$\dot{\omega} = -\left(\frac{2|\mathbf{m}|^2 sin^2\alpha}{3c^3 I}\right)\omega^3 \tag{1.3}$$

The above equation has the form of,

$$\dot{\omega} \propto \omega^n \tag{1.4}$$

where n is known as the **'braking index'** of the pulsar, and for pure magnetic dipole radiation n = 3. The value of n measured for a few pulsars are slightly less than 3, suggesting that perhaps not all the angular momentum is carried by dipole radiation. Assuming that the spin-periods of pulsars when they are born are significantly fast, the **characteristic age of the pulsar,** τ, can be found by integrating equation(1.4), which gives,

$$\tau = \frac{P}{(n-1)\dot{P}} \tag{1.5}$$

where $\dot{P}$ **is the period derivative.** For n=3, $\tau = P/2\dot{P}$, is the characteristic age assuming dipole radiation. For normal pulsars the typical **P** measured is about 10^{-15} ss^{-1} and **P** $\sim$ 1 s which give characteristic ages of a few million years. Millisecond pulsars have $\dot{P}$ of about 10^{-19} ss^{-1}, with characteristic age of order a billion years. The millisecond pulsars are thought to have been spun up to their present periods by accretion of material from their binary companions. The **magnetic field,** B_s, for a pulsar can be calculated using equation (1.2). For a magnetic dipole the field at a distance r from the dipole center along the dipole axis is given by $|\mathbf{m}|/r^3$. Substituting $B_s = |\mathbf{m}|/R^3$ in equation (1.3) the magnetic field at the neutron star surface is given by

$$B_s \doteq \left(\frac{3c^3 I}{8\pi^2 R^6 sin^2\alpha}\right)^{1/2}\sqrt{P\dot{P}} \tag{1.6}$$

Accurate measurements of the mass of a neutron star (M) can be obtained for a neutron star in a binary with a companion of known mass. Such measurements indicate **that the mass of a neutron star** is **–1.4** M$_\odot$ (Joss & Rappaport 1976). The typical

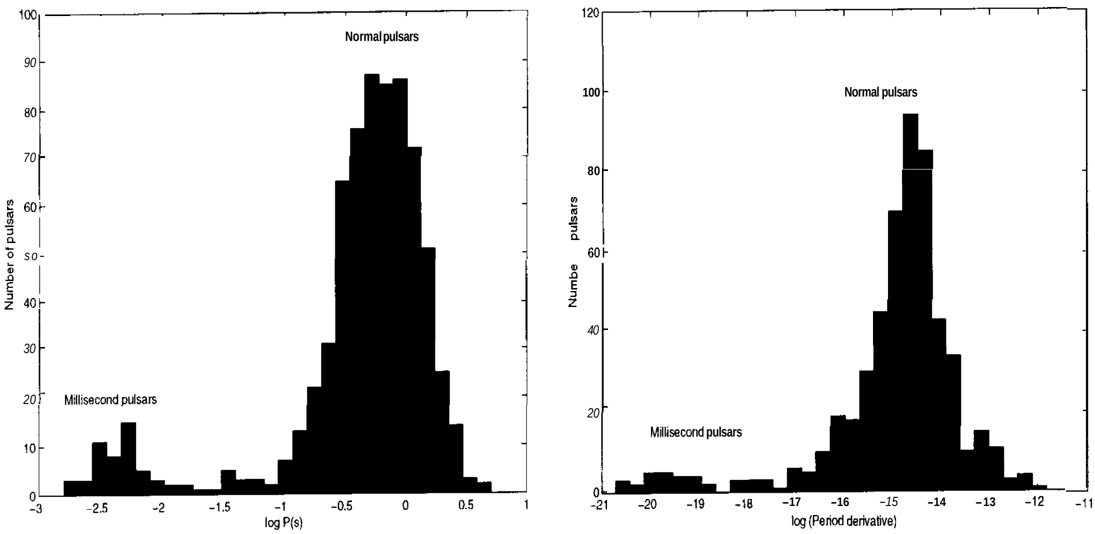

Figure 1.2: Distribution of periods of 706 pulsars, and period derivatives for 538 pulsars. The distributions has two distinct regions namely the millisecond pulsars and the normal pulsars.

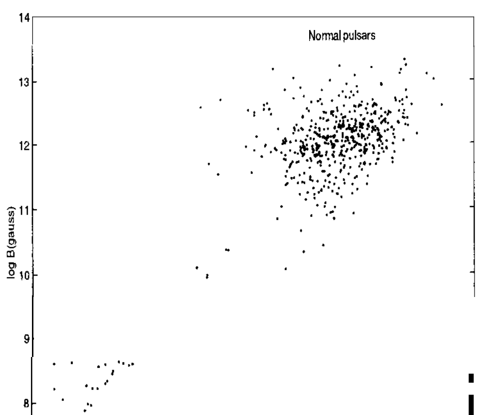

Figure 1.3: Surface magnetic field versus period for 538 pulsars.

value of the **radius of a neutron star** is $R \approx 10$ km, which is the value obtained for a neutron star of average density 10^{14}gcm^{-3} and is also predicted by most equations of state. Thus the **moment of inertia, $\mathbf{I} = \mathbf{MR}^2$** $\sim 10^{45}\text{gcm}^2$. Putting these values in equation (1.6), we get,

$$B_s = 3 \times 10^{19}\sqrt{P\dot{P}} \text{ gauss} \tag{1.7}$$

The above expression is derived with $\alpha = 90°$ from vacuum dipole torque (eq. 1.3, 1.6). Torque exerted by outgoing particle stream is expected to have a different dependence on a (Goldreich & Julian 1969). Recent work (Bogovalov 1997) appears to suggest that the net torque is given by the same functional form as equation (1.3), but without the a dependent factor. Equation (1.7) is thus expected to be a fair estimate of the magnetic dipole field irrespective of the magnetic inclination α.

In figure (1.3) magnetic fields calculated using equation (1.7) for 538 pulsars is shown as a function of pulsar period. The points segregate into two distinct groups, the millisecond pulsars having magnetic fields $\sim 10^8$ gauss and the normal pulsars having $\sim 10^{12}$ gauss. It is thought that the magnetic field of a normal pulsars decavs considerably during the process of getting 'recycled' into millisecond pulsars by accretion driven spin-up. Theoretical studies concerning evolution of magnetic fields in pulsars have linked the evolutionary sequence from normal to millisecond pulsars, though the subject is very much a matter of debate. The magnetic field of pulsars are also important in understanding the emission mechanism of pulsars.

1.3 Radio pulses from pulsars

Pulsars are prolific radio emitters and exhibit broad band emission from as low as 30 MHz to as high as 80 GHz. In figure (1.4) a schematic diagram for a typical pulsar spectrum is shown. Detailed study of the radio spectrum (Malofeev et al. 1994) indicates a low frequency turn-over of the spectrum around 100 MHz. The spectrum is well characterized by a power law above and below the turnover frequency, where the average flux at a given frequency $S_\nu \propto \nu^{-\eta}$, η being the spectral index. Above 100 MHz the spectrum **is** rather **steep** with mean **$\eta \sim 1.8$.** In some case there is a

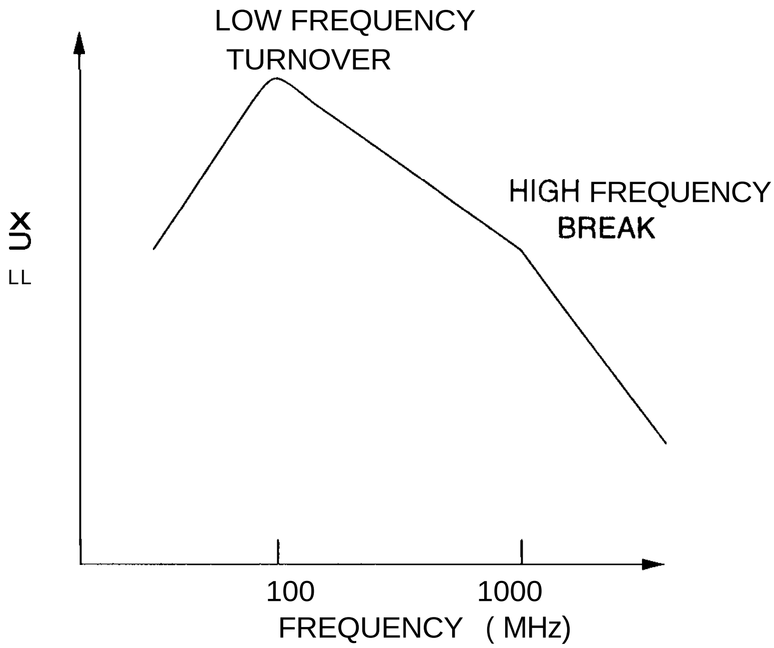

Figure 1.4: Schematic representation of a typical spectra observed in radio pulsars.

break in the spectrum observed at high frequencies (>1 GHz) and the spectrum above turn-over can be split into two power laws (Malofeev et al. 1994, Lorimer et al. 1993). At verv high frequencies above 34 GHz there are indications that for a few pulsars the flux tends to rise (Kramer 1995), though this fact has not been concliisively proven.

The spectral radio luminosity of a pulsar (L_ν) is defined using S_ν and the distance (D) to the pulsar as,

$$L_\nu \equiv S_\nu D^2 \quad \mathrm{mJy\ kpc^2} \tag{1.8}$$

(see Manchester & Taylor 1977). Using the average flux at 400 MHz, the typical radio luminosities found are of the order of 10^{24} erg/s to 10^{28} erg/s. The spin-down luminosity calculated as *Iww* lies typically in the range of 10^{30} erg/s to 10^{38} erg/s. This suggests that a very small fraction of the total energy release from the star is actually emitted in the radio band. The brightness temperatures calculated for pulsars are in the range of 10^{23} K to 10^{26} K. Such high brightness temperatures suggest that the radio emission originates in a coherent process.

1.3.1 Single pulses

The typical duty-cycle of pulsed radio emission from pulsars is ~1.5 to 6%, corresponding to 5° to 20° of angular rotation (a complete period corresponds to 360° angular rotation of the star.) The individual pulses show large variety in their shape, intensity and polarization properties. In figure (1.5) a sequence of 50 single pulses of PSR B0329+54 observed simultaneously at 322.5 MHz using the Ooty Radio Telescope and 1.41 GHz using the Lovell Radio Telescope are shown. The enormous variations from pulse-to-pulse are clearly evident. Also note that the variations are highly correlated between the two frequencies, implying broad band correlated emission features. The individual pulses (Fig. 1.5) often comprise of several gaussian like features, known as subpulses which are understood as basic units of emission (Ruderman & Sutherland, 1975). Subpulses tend to wander around, drifting in longitude from pulse to pulse, mostly in some correlated manner. The width of the subpulses in pulsars varies from 2" to 10" in longitude. The full width at half maximum of the subpulse does not seem to depend on frequency. The widths of subpulses are often correlated with their intensity in a manner such that stronger subpulses tend to have narrower widths. In some cases, the subpulses of successive pulses are seen to drift across the pulse window. Such drifts are interpreted as the emission sources (also known as sparks) moving in a circular motion around the pulsar polar cap. The line-of-sight of the observer cuts through the pulsar beam thus sampling an intensity pattern in a given pulse. In successive pulses the intensity pattern drifts illuminating a different set of longitudes, and an apparent drift pattern is observed (Drake & Craft 1968, Deshpande & Rankin 1999). In figure (1.5) pulse number between 12 to 15 suddenly seem to have reduced drastically in intensity and pulse number 15 have switched off completely. This phenomenon is known as nulling (Rankin 1986 and references therein). Nulling can even last for hundreds of pulses. As clearly visible in the figure, nulling can occur simultaneously at different frequencies. Drift rate in drifting subpulses seems to reduce significantly during a null state.

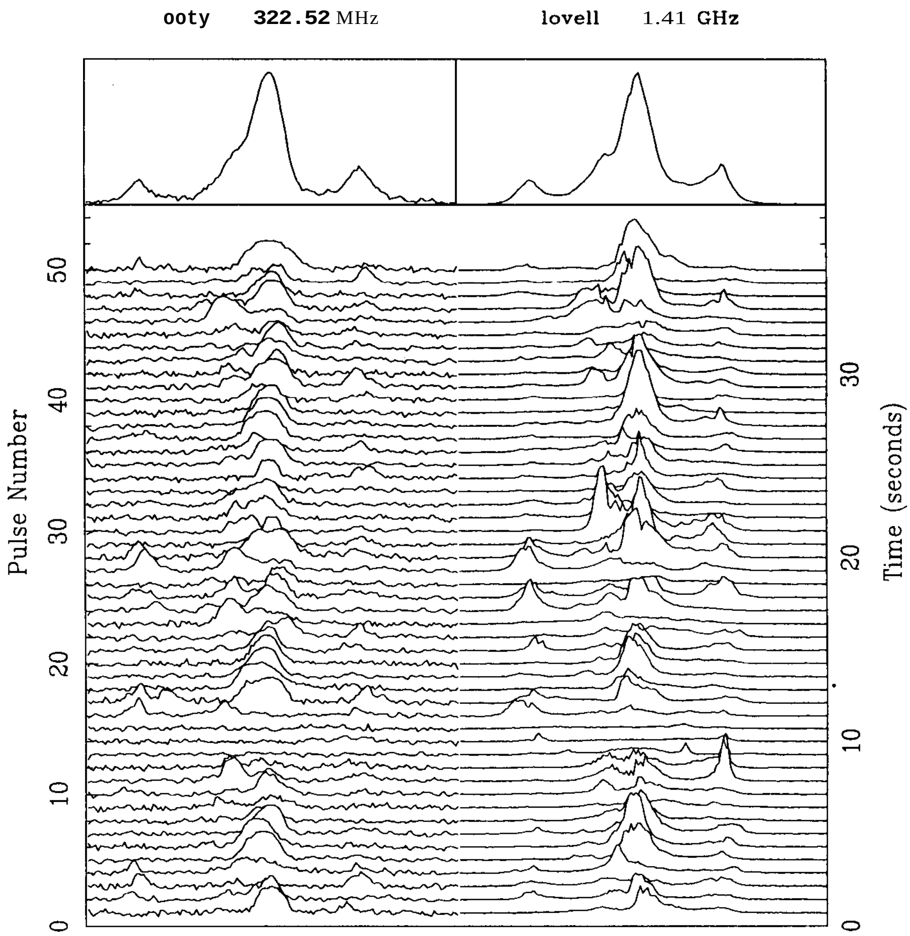

Figure 1.5: A sequence of 50 single pulses of PSR B0329+54 observed simultaneously using the Ooty Radio telescope at 0.3 GHz and the Lovell telescope at 1.4 GHz. Observations were done as a part of the European Pulsar Network simultaneous observation campaign. The horizontal axis is the pulse phase and the vertical axis refers to the

1.3.2 Integrated Pulses

Though the individual pulses show remarkable variety in their pulse shapes, the integrated average pulse profile, obtained by averaging over thousands of periods shows a remarkably stable shape. In figure (1.5) the average profile averaged for 50 pulses is shown on the top panel. Techniques studying the stability time scales (Helfand et al. 1975, Rathnasree & Rankin, 1995) of pulse profiles suggest that typically 1000 to 3000 pulses are required to form a stable shape. For PSR B0329+54 the stability time-scale is about 2500 periods. The integrated pulse profile is rather unique and pulse shapes observed even over decades does not seem to change. Integrated pulse profile for a given pulsar is a rather characteristic feature of the pulsar itself so much so that the shape itself can be used to identify the pulsar. Integrated pulse shapes are generally composed of one to as many as 7 components, with each component typically characterized by a gaussian shape. The components in general represent the longitudes of preferential occurrence of subpulses. According to the classification scheme suggested by Rankin(1983a), a single component profile can either be a core (S_t) or a conal single (S_d). The two component profile is a conal double (cD) and the three and four component profiles are conal triples (cT) and conal quadruples (cQ) respectively. Pulsars with more components are classified as multiples (M). The stability of profiles hints towards a rather stable and repetitive emission mechanism.

While the pulse shape of the average profile is extremely stable, sometimes a pulsar for several hundreds of pulses exhibits an entirely different profile shape and then returns to its original shape. This phenomenon is known as mode changing. The frequently occurring mode is called the normal mode while the less frequent one is known as the abnormal mode. An example for such mode changing phenomenon for PSR B0329+54 is shown in figure (1.6).

The integrated pulse shapes are frequency dependent. The pulse width (usually defined as the half power points of the outer components) shows a gradual decrease with increasing frequency. In some rare cases however the width at a lower frequency is smaller than that at a higher frequency (Rankin 1983b).

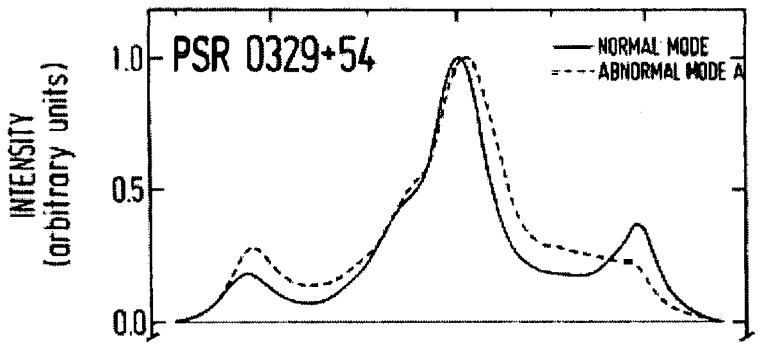

Figure 1.6: Example of mode changing in PSR B0329+54 at 1.7 GHz (Bartel et al. 1982). The continuous line is the 'normal' mode and the dashed line is tlie 'abnormal' mode.

1.4 Coherent Curvature Radiation

The proposed emission mechanism for pulsar radiation is the coherent curvature radiation. A charged particle moving in a curved trajectory feels an acceleration in the direction of the radius of curvature, κ as shown in figure (1.7). If the particle moves relativistically with Lorentz factor γ, the emission will be beamed in the direction of motion of the particle and the emission beam will have an angular cone half-width of $1/\gamma$ (cf. Fig. 1.7). An observer sampling different parts of the emission cone, will find the emission to be circularly polarized at the edges of the cone while at the center the emission is linearly polarized (cf. Fig. 1.7). The circular polarization in such a case will change handedness as it crosses zero at the center of the cone. The linear polarization will be in the direction of the field line curvature. It is clear from the geometry involvetl that curvature radiation would have the same properties as those of synchrotron radiation with pitch angle $\pi/2$. The polarization signatures calculatetl by Solokov & Ternov (1968) for synchrotron radiation viewed a.t an angle to the plane of motion is shown in figure (1.7), and these apply in the case of curvature radiation too.

The incoherent power (P_c) radiated by curvature radiation is given by:

$$P_c = \frac{2}{3}\frac{e^2 c}{\rho^2}\gamma^4 \quad \text{ergs/s} \tag{1.9}$$

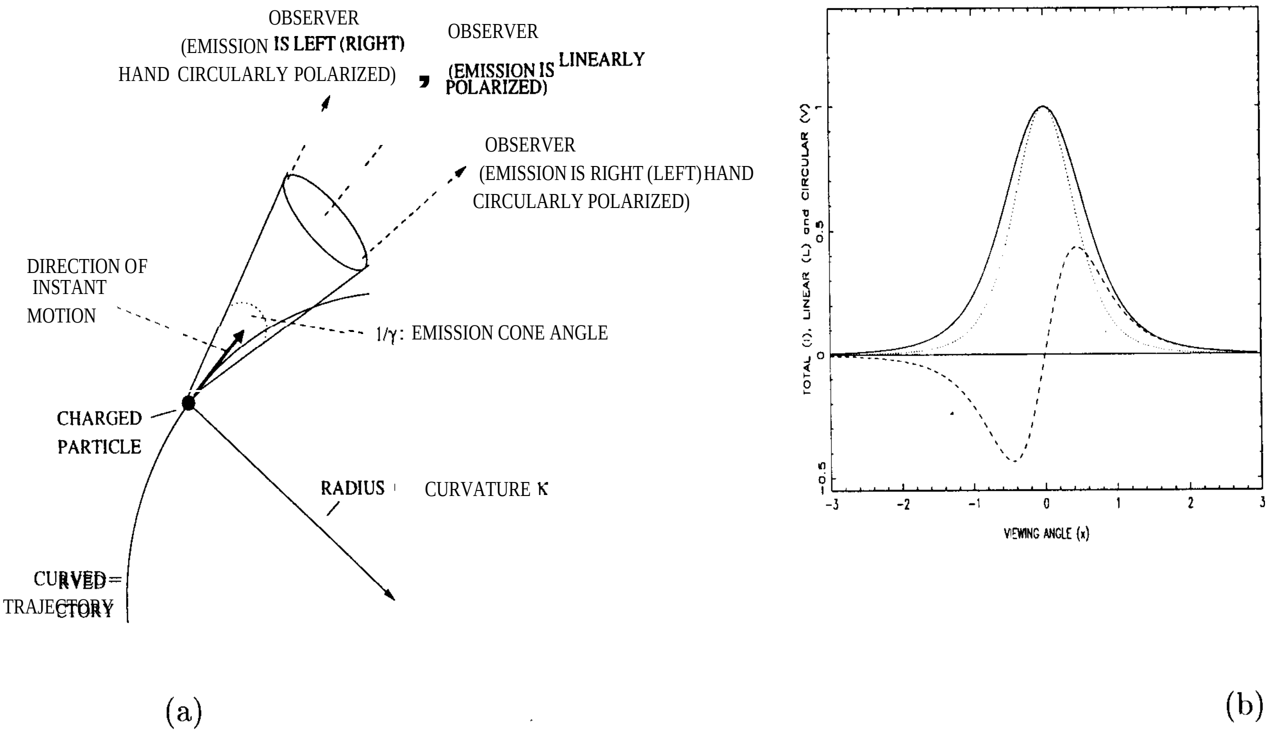

Figure 1.7: In panel (a) the schematic picture for curvature radiation is shown. Charged particles moving along curved trajectories emits in the direction of motion with an $1/\gamma$ half-width emission cone. The polarization received by the observer at different viewing angle is shown. In panel (b) the intensity of total **I** (continuous line), circular polarization V (dashed line) and linear polarization L (dotted line) as a function of normalized viewing angle (x) due to synchrotron radiation is shown. Following Solokov & Ternov (1968), $\mathbf{I} = (7 + 12x^2)/(1 + x^2)^{7/2}$ and $V = 64x/\pi\sqrt{3}(1 + x^2)^3$ and $L = \sqrt{I^2 - V^2}$.

where e is the charge of the accelerated particle and c is the velocity of light. The characteristic frequency (ν_c) of curvature radiation is:

$$\nu_c = \frac{1}{2\pi}\frac{3c}{2\kappa}\gamma^3 \quad \text{Hz} \tag{1.10}$$

The spectrum rises as $\nu^{1/3}$ up to ν_c and above this the spectrum decreases exponentially.

The incoherent power emitted by single particle curvature radiation (equation 1.9), however, is insufficient to explain the observed high brightness temperatures (cf. section 1.3) in pulsars. Such temperatures can be achieved by invoking coherent emission mechanism where several particles bunch together to emit coherently. As a result the emitted power is amplified sufficiently to be able to explain high brightness temperatures. However, it should be mentioned that the physics of such hunching mechanism is still unclear.

1.5 Polarization Behaviour

Pulsar emission is highly linearly polarized with the degree of linear polarization being as high as 70% to 80%. Radhakrishnan & Cooke (1969) observed that the position angle of the linear polarization within the pulse window rotates smoothly as a function of longitude in a S-shaped fashion (refer Fig 1.8). This smooth S-shaped curve is a characteristic feature of almost all known pulsars, hinting strongly towards an underlying dipolar magnetic field. The steepest gradient in the position angle curve occurs typically at the center of the pulse profile arid the curve is symmetrically placed about this point. The curve does not change significantly with observing frequency, indicating that the observed swing is intrinsic to the pulsar emission and riot a result of propagation. The total extent of tlic curve is typically about 180° and can decrease due to the narrowing of the profile.

The origin of the S-shaped curve can be understood by invoking curvature radiation (cf. section 1.4). Charged particles moving relativistically along the open dipole field lines emits curvature radiation beamed in the forward direction along tlic instantaneous motion. An observer would however see the radiation due to charged particles which are accelerated linearly along the projected magnetic field lines in the sky and thus the

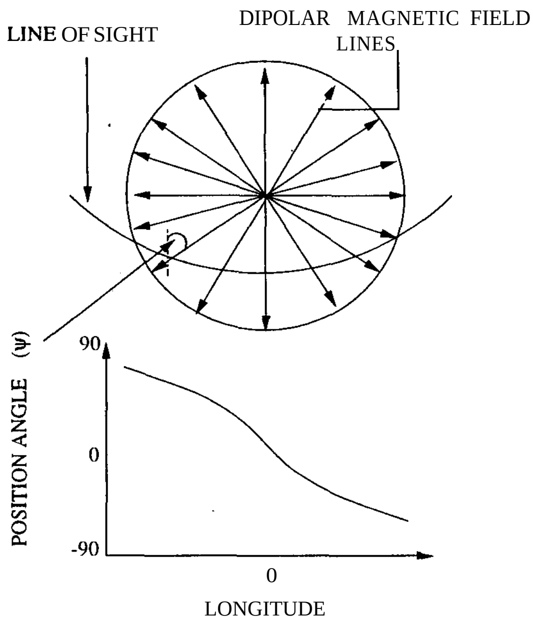

Figure 1.8: The above schematic diagram shows the polarization position angle (Ψ) curve (in the bottom panel) obtained as the line-of-sight of the observer crosses the pulsar beam (in the top panel). The characteristic 'S' shape of the position angle is due to the projected dipolar magnetic field lines on the sky as predicted by the rotating vector model (Radhakrishnan & Cooke, 1969).

radiation observed will be linearly polarized along the projected magnetic field. If γ is sufficiently large, tlie emission cone width will be extremely narrow and as a function of the viewing angle the observer will essentially see linearly polarizecl emission. The characteristic S-shape, as shown schematically in figure (1.8), is typical to dipolar magnetic field geometry. For a different magnetic field structure, which might arise due to the presence of higher multipoles in the emission region, the S-shaped curve is expected to develop kinkiness (refer chapter 4).

Subpulses are generally more highly polarized than the integrated pulse (Taylor & Huguenin, 1975). This suggests that the subpulses of individual pulses have variability of polarization which gets averaged out in the integrated profile. In an individual subpulse tlie total position angle swing can go up to 30°, though this fact is not conclusively proven. The other manifestation of the linear polarization arises as an orthogonal position angle jump in the position angle traverse. The linear polarization in certain parts of the profile flips by 90°, and instead of the smooth S-shaped curve, there are discontinuous steps observed. In figure (1.9) an example of the orthogonal flip is shown for PSR, B1133+16. The flips in some pulsars, however, are observed to be non-orthogonal, with the two position angle tracks being separated bv either more or less than 90" (Backer & Rankin, 1980). It is also observed that at the same longitude radiation in different modes are seen at different times.

Towards the center of the pulse profile, typically below the core component, circular polarization is observed. In integrated profiles the degree of circular polarization is about 20% of tlie total intensity which can often reach 50% towards the center of the profile. There is a sense reversal of circular polarization observed which occurs usually once in a given profile. Mode switching in circular polarization is not observed frequently, however in some cases circular polarization is seen to change handedness (Cordes et al, 1978).

The orthogonal mode switching of the position angle as seen in pulsars is rather mysterious, and there is no good understanding as yet of tlie mechanism responsible for this. Clieng & Ruderman (1977), interpret this as a propagation effect whereas Michel (1987) considers the possibility that the effect is geometrical in origin.

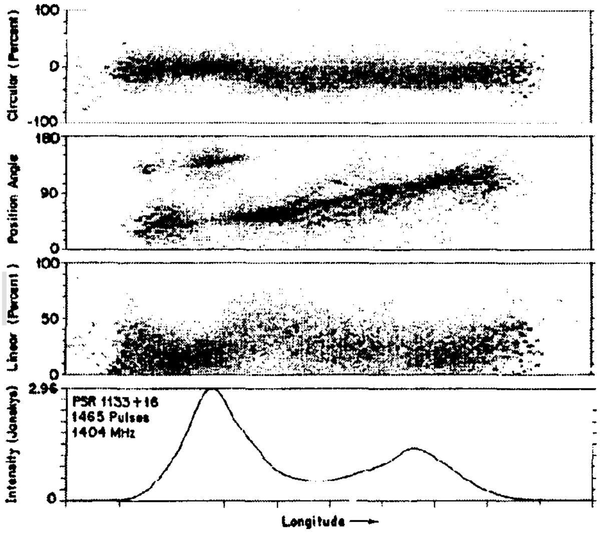

Figure 1.9: Polarization characteristics of PSR B1133+16 from Stinebring et al, 1984. The 'S' shaped variation of the position angle Ψ is clearly visible. Also note the orthogonal flips in the position angle as discussed in section 1.5.

1.6 Phenomenological Models

A single theory which is able to explain the observed radio emission of pulsars is yet to be found. The pulsar problem is that of a highly conducting sphere, rotating in a strong dipole magnetic field, located at the center of the star, with the region exterior to the sphere initially being vacuum. Goldreich and Julian (1969), assuming that the magnetic axis is aligned with the rotation axis, showed that the neutron star is capable of generating very high voltages $\sim 10^{16}$ volts. Further assuming that the neutron star is a copious supplier of charged particles, the strong electric field is able to pull out charged particles from the stellar surface. The strong magnetic field makes the particles move along the field lines into the surrounding vacuum, until the region is filled with plasma, forming the magnetosphere. In a steady state the magnetospheric plasma would co-rotate with the star.

Co-rotation of the magnetospheric plasma, however, can be maintained only up to a boundary where the co-rotation speed is equal to the speed of light. The distance up to which co-rotation exists is given by,

$$R_{\mathrm{L}} = \frac{c}{\omega} = 4.8 \times 10^9 \left(\frac{P}{1 \text{ sec}}\right) \text{ cm} \tag{1.11}$$

R_{L} is known as the radius of the **light cylinder** (refer Fig. 1.1). The light cylinder divides the region of the dipolar magnetic field lines into two regions, namely the closed field lines and the open field lines. The closed field lines are defined as the field lines which close within the light cylinder, while the open ones do not. Particles flowing out through the open field lines can cross the light cylinder and finally get deposited into the interstellar medium. Continuous supply of charged particles from the star along the open field lines thus keeps the emission region active. Particles which are trapped in the closed field lines co-rotate with the neutron star,forever, and do not participate in pulsar radiation. The radio emission from pulsars is assumed to originate primarily within the cone defined by the open field lines (Fig. 1.1).

The most successful model which has emerged over the years, explaining the radio emission observed, is the hollow cone model initially proposed by Ratlhakrishnan & Cooke (1969). Subsequent workers (e.g. Komesaroff 1970, Oster & Sieber 1976, Rankin 1993a,b, Gil et al. 1993) have considerably refined the hollow cone model. In the hollow cone model the beam of pulsar radiation is assumed to be in the form of a hollow cone centered around the axis of the magnetic dipole. The cone is hollow as the intensity distribution of the cone is maximum near the edge of the cone, falling off gradually towards the center. In the case of a single hollow cone, when the observers line-of-sight (LOS) grazes through the edge of the cone, a conal single S_d profile is observed. For an LOS cutting the inner parts of the cone, conal double (cD) profiles are observed. However to explain the variety of pulse shapes observed a single hollow cone model is insufficient. As early as 1976, Oster & Sieber invoked the idea of a 'nested cone' structure around the magnetic axis, which suggests multiple cones of emission instead of a single hollow cone. Apart from the conal components observed in pulsars, there is a central component which is frequently observed. To accommodate this component in the hollow cone model, Backer (1976) introduced a pencil-beam of emission close to the magnetic axis which was later given the name 'core' by Rankin (1983). The core component is associated with significant reversal of handedness in circular polarization and no drifting subpulse pattern. The spectral index of the core is steeper than that of the conal components (Rankin, 1983a, Lyne & Manchester 1988, Kramer et al 1994). Rankin (1993a,b), extended the hollow cone model to a double hollow cone with a central core component which could successfully explain the five component profiles observed. In figure (1.10) the schematic diagram illustrating the hollow cone model is shown. The number of components observed depends on where the LOS passes through the hollow cone. The case of a single hollow cone can be intuitively understood by invoking curvature radiation. Charged particles flowing along the open field lines emits curvature radiation which depends inversely on the square of the radius of curvature of the field lines. In the case of a dipole, the radius of curvature decreases as one moves away from the dipole center. Thus the power emitted at the edges of the cone is higher and gradually decreases towards the center. The central field line which defines the magnetic axis has infinite radius of curvature and the power goes to zero. This picture is too simple to be able to explain the multiple cone structure in pulsars. The only attempted explanation so far available in the literature is that of Shier (1992), where the inner cone of the double cone structure is attributed to be reflection from the magnetospheric plasma. However, this argument is rather hand-waving. The most difficult problem is to explain the origin of the core emission. Rankin (1993a) suggested that the core component is due to emission from particles with low lorentz factor, occurring very close to the stellar surface and filling the whole polar cap.

There is another viewpoint primarily put forward Lyne & Manchester (1988), which differs from the idea of the nested cone structure of the pulsar emission region. According to them, the pulsar beam is filled with emission patches in a random fashion. The LOS crosses these random emission patches to give rise to the components in the pulsar (refer Fig. 1.10). In this picture the core and cone emission are attributed to the same emission mechanism (also see Gil et al. 1993). This picture, however, is not supported by observations and should not be taken seriously. In chapter **2** we revisit the problem of the shape of the pulsar emission beam, and convincingly argue in favour the nested cone structure (Gil et al. 1993, Kramer et al. 1994, Rankin 1993a).

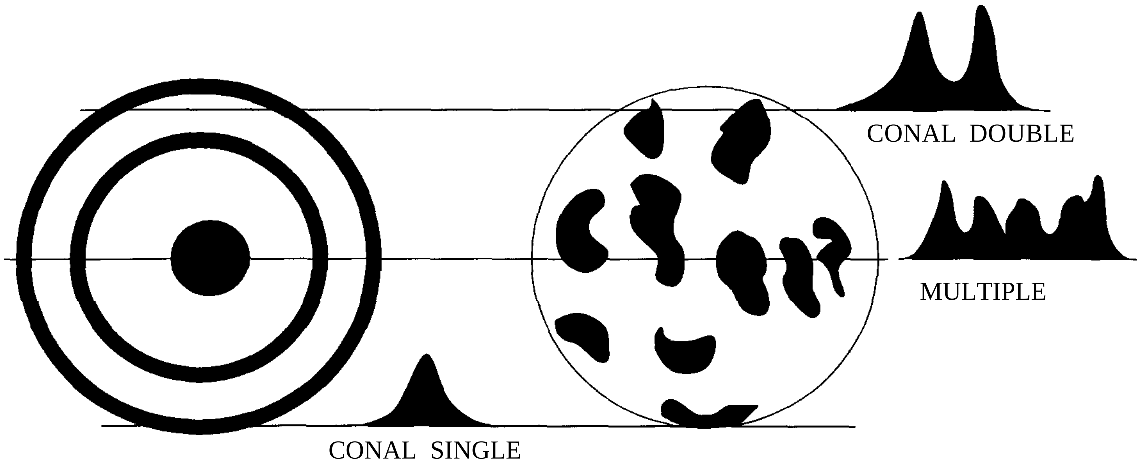

Figure 1.10: A schematic representation of the hollow cone model versus the patchy model of the pulsar beam. Different lines of sight cutting various parts of the beam can give rise to the observed pulse shapes.

For a dipolar field line, $\sin^2(\theta)/r$ is a constant, where (r,0) are spherical polar co-ordinates. The last open field line which is tangential to the light cylinder is defined by $\theta = 90^\circ$ and $r = R_\mathrm{L}$ at the light cylinder. Thus for the same field lines the two points (r,θ) and $(R_\mathrm{L}, 90^\circ)$ can be equated, which gives

$$\sin\theta = \sqrt{\frac{r}{R_\mathrm{L}}} = \sqrt{\frac{2\pi r}{cP}} \tag{1.12}$$

The same field line at the stellar surface is defined by the polar co-ordinates (R,θ_p). At the edge of the polar cap (co-ordinates R,θ_p), the field line is inclined to the radius vector by $\tan^{-1}(0.5\tan\theta_\mathrm{p})$. The opening angle ρ, defining the direction of the emitting photon is thus given by,

$$\rho = \theta_\mathrm{p} + \tan{-'} \left(\frac{\tan(\theta_\mathrm{p})}{2}\right) \tag{1.13}$$

In practice θ_p and p are small and we obtain the following two important results:

1) The angular diameter of the polar cap using equation (1.12) with polar co-ordinate (R,0,) is,

$$2\theta_\mathrm{p} = 2\left(\frac{2\pi R}{c}\right)^{1/2} P^{-1/2} \tag{1.14}$$

2) The angular width p of the beam is,

$$2\rho = 3\theta_\mathrm{p} \tag{1.15}$$

The radius of the polar cap (r_p) is $\sim \mathrm{R}\sin\theta_\mathrm{p}$ thus giving,

$$r_\mathrm{p} \approx \sqrt{\frac{2\pi}{c}} R^{3/2} P^{-1/2} \tag{1.16}$$

Assuming a value of $\mathrm{R} = 10$ km and $\mathrm{P} = 1$ sec, the polar cap radius is about 150 m.

There are two strong pieces of evidence suggesting that pulsar emission arises from dipolar open field lines containing the magnetic axis. The first one comes from investigation of profile widths. Let us assume the emission originates from a distance r from the center of the star with the last open field line at an polar angle θ. Using equation (1.12) and (1.13) and replacing θ_p by $\mathbf{0}$ in equation (1.13), we obtain,

$$\rho = \frac{3}{2}\theta = 3\sqrt{\frac{\pi r}{2c}} P^{-1/2} = 1.24^\circ r_6^{1/2} P^{-1/2} \tag{1.17}$$

where ρ is in degrees and $r_6 = r/10^6$ cm. Independently ρ can be obtained from observations if the angle α between the rotation axis and the magnetic axis, the angle β between the magnetic axis and the LOS and the width ϕ of the pulse profile are known (refer Chapter 2 eq. 2.6). Such estimates of ρ clearly show the $P^{-1/2}$ dependence as given by equation (1.17), thus strongly arguing in favour of the dipolar geometry (Rankin 1993a, Gil et al. 1993, Kramer et al. 1994). The other evidence arises from the position angle sweep curve of the linear polarization. In most pulsars careful single pulse studies clearly shows the S-shaped swing of the position angle across the pulse profile which is a characteristic feature of a dipolar field (refer Chapter 3, and for an excellent review Radliakrishnan 1992).

It is of great importance to understand where the radio emission originates in pulsars. The most important clue to this comes from the pulse width measurements for a range of frequencies. Almost for all pulsars, it is seen that the widths of pulses observed at lower frequencies are larger than those at higher frequencies. The simplest explanation for this is that the altitude r at which the emission originates from the dipolar open field lines. is a function of frequency. The opening angle of the last open field lines decide the pulse width. As the field lines flare out with increasing distance from the star, it is thought that lower frequencies (larger widths) originate at higher altitudes while higher frequencies (smaller widths) originate at lower altitudes.

This is known as the **radius** to **frequency mapping** in pulsars. Assuming dipolar geometry and that all emission at a given frequency arises at the same height from the stellar surface, the absolute height r can be found geometrically (Rankin, 1993): from equation (1.17) we get

$$r = 10\rho^2 P/(1.24^\circ)^2 = 6.67\rho^2 P \tag{1.18}$$

where r is in km, ρ in degrees and P in seconds. Emission heights calculated using the above equation suggest that the radio emission arises within 10 times the stellar radius (Rankin, 1993). Such arguments applied to the inner cone and the outer cone suggest that the two cones arise from two different heights, and the emission height of the inner cone is less than the emission height of the outer cone onlv by a factor of two. Another method that can be employed to estimate the radius to frequency mapping in pulsars comes from timing measurements. If emission arises at different heights, the signal which arises from a higher altitude will arrive earlier than the signal from a lower altitude. Simultaneous, milltifrequency measurement of the arrival times of pulses should clearly show this delay. Such studies suggest, that the cniission region is rather compact, (Kramer et al. 1994). However, this method yields only the extent, of tlie emission region, and not absolute heights.

1.7 Emission Models

Theoretical models for pulsar radio emission should focus on explaining primary issues like high radio power output, the observed narrow pulses and the spectrum. A complete introduction to emission mechanism is beyond the scope of this discussion here. Here we briefly deal with the emission model put forward by Ruderman & Sutherland (1975) and discuss the salient features of the model. Though not free from defects, Ruderman & Sutherland (1975, hereafter RS throughout tliis section) is the most widely used model, primarily because it can explain a large body of observations and also is rather user friendly.

RS considered a neutron star with its spin axis and magnetic axis being aritiparallel to each other. They use the result obtained by Goldreich & Julian (1969), that during a steady state charged particles are pulled out from the stellar surface and fill up the magnetosphere. The solution thus obtained is that, in the whole magnetosphere there exist two types of charges, separated by a region defined by the line $\cos\theta = \pm 3^{-1/2}$, where θ is the polar angle with respect to the rotation axis. The region above the polar cap is filled with positive charges and along the equator with negative charges. Charges are pulled out till the force free condition is satisfied, i.e. $\vec{E}.\vec{B} = 0$, where $\vec{E}$ is the electric field. In regions of closed field lines the charges get trapped and co-rotate with the star. However, loss of charge takes place in regions of open field lines and this causes $\vec{E}.\vec{B} \neq 0$. In such regions a parallel component of $\vec{E}$ will be generated along $\vec{B}$ which will further try to pull out positive charges (ions) from the stellar surface. RS claimed that under such strong magnetic fields the binding energy of ions to the star is extremely high, and thus they cannot be easily pulled off. Lack of supply of ions will produce a 'gap' above the polar cap, across which a strong potential difference will be generated. For a gap distance h the potential difference AV is given by $\Delta V = wB_s h^2/c$ (equation 16 of RS), valid for $h << r_p$. Gap height h will grow at the speed of light, and since $\Delta V \propto h^2$, the potential difference will increase rapidly. Beyond a certain ΔV the gap will be discharged by an avalanche of electron-positron pairs. For a pulsar with $B_s \sim 10^{12}$ gauss, $w = 2\pi$ sec^{-1} and $h \sim 10^3$ cm, the potential difference is $\Delta V \sim 10^{12}$ volts. It was shown by RS that h for a given pulsar depends on its magnetic field, its period and on the radius of curvature of the magnetic field lines near the stellar surface. h is however weakly dependent on the radius of curvature and RS assumed the radius of curvature of the last open field line near the stellar surface to be 10^6 cm which is ~ 100 times smaller than the dipolar value. They argue that it is expected that the magnetic field near the stellar surface to be multipolar, which gives the reduced value of the radius of curvature.

Slow down of pulsars has the interesting consequence that ΔV would reduce, and thus to maintain discharges, h would grow. However, as h approaches r_p the relation for ΔV breaks down, and the electric field in the gap falls off exponentially. As the potential difference drops below 10^{12} volts, discharges are no longer possible. The critical period above which discharges stop is given by,

$$P_{crit} = 1.7 B_{12}^{8/13} R_6^{21/13} \kappa_6^{-4/13} (15\chi)^{-2/3} \text{ sec} \tag{1.19}$$

where, B_{12} is the magnetic field in units of 10^{12} gauss, R_6 is the radius of the star in units of 10^6cm, κ_6 is the radius of curvature in units of 10^6 cm and χ is a ratio of the order of 1/15. Stoppage of discharges, in the RS model, causes the death of a pulsar, which happens as the pulsar slows down with age and the period lengthens beyond P_{crit}. This in turn explains why we don't see very long period pulsars (for example P > 10 sec).

The electron-positron pairs produced in the gap, known as primary particles, move along curved field lines to produce curvature radiation photons with energies in excess of $2mc^2$. Such energetic photons in strong magnetic fields produce further cascade of secondary and tertiary particles with energies much less than that of the primary particles. At altitudes of 10^6 cm, which is above the gap, the lorentz factor of the particles are ~ 800, and the underlying magnetic field is dipolar. The characteristic frequency producetl by such particles fall in the radio frequency range, which is observed. This model by itself, however, does not provide a mechanism for particle bunching required to explain the coherence of radio radiation. Pulse shapes are most probably decided by the way the sparks populate the polar cap. The polarization characteristics are decided by the magnetic field lines from where the emission originates (Radhakrishnan & Cooke, 1969). However, since the predicted lorentz factors are extremely high, the emission will be beamed in the form of a pencil, and no circular polarization is predicted by the RS model.

The essential feature of the RS model is that tlic ions on the neutron star surface have strong binding energy, and thus a gap is able to form. This issue however is rather controversial, as recent estimates (Hillebrandt & Miiller, 1976, Flowers et. al. 1977, Kössl et al. 1988) show that the binding energy is not high enough to do so. Nevertheless, to produce the observed eriiission, an acceleration mechanism is essential and further to explain the coherent emission a large number of particles are necessary. What makes the RS model promising is that it provides both these. Recently, Muslimov & Tsygan (1992) have shown that the effects of general relativity can produce the required accelerating potential even in absence of a 'gap' near the surface. However, an effective theory is yet to emerge.

1.8 Neutron star Interior

Neutron stars are extremely dense objects with masses comparable to the mass of the sun, but with a radius of only 10 km. The average density of a neutron star, $\gtrsim 10^{14}$ gcm^{-3}, exceeds the density of nuclear matter. Most of the neutron star is composed primarily of a sea of neutrons ($\sim$99%) with a small admixtiire of protons and electrons ($\sim$1%), as dictated by β-equilibrium at such high densities. Conditions near the center of neutron stars are uncertain as the equation of state at these densities ($\sim 10^{15}$gcm^{-3}) cannot be directly derived from terrestrial measurements. The low density outer parts of the neutron star, however do contain nuclei, albeit neutron-rich. This region is commonly referred to as the 'crust' of the star. Depending on the overall state of matter, we divide the neutron star into primarily three regions namely the outer crust, the inner crust and the core as shown in figure 1.11. It should be noted that the interior structure of the neutron star strongly depends on the equation of state.

The **outer crust** lies within the density regime of $7.86 < \rho_{ns} < 4 \times 10^{11}$ gm/cc. The matter consists of degenerate ions and electrons and has a depth of a few hundred meters. For ρ_{ns} greater than 10^6 gm/cc the electrons constitute a strongly degenerate relativistic ideal gas. The atoms are fully ionized by the electron pressure and are bare atomic nuclei at densities greater than 10^4 gm/cc. For $\rho_{ns} > 10'$ gm/cc, the electron fermi energy approaches the MeV energy range, when the protons undergo an inverse β-decay, thus giving rise to neutron-rich nuclei in the crust. The pressure contributions at these densities is primarily due to the free fermi degenerate electron gas pressure. However, here electrostatic corrections to the equation of state become important as the positively charged ions are not uniformly distributed, thus decreasing the electron pressure. Taking such considerations into account the equation of state in this density regime has been calculated by Baym, Pethick and Sutherland (1971).

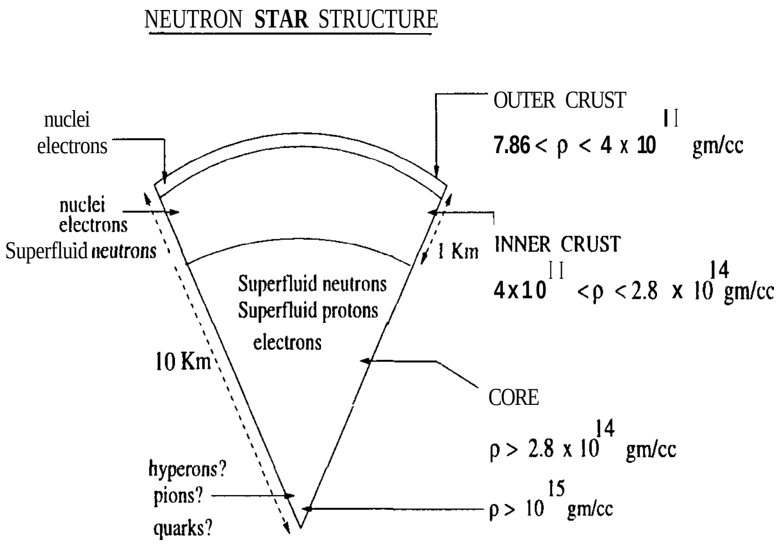

Figure 1.11: Schematic representatiori showing tlie interior of the neutron star

The **inner crust** (Fig.1.11), in tlie density range 4 x 10^{11}gm/cc to 2.8 x 10^{14}gm/cc dominates the crustal width which may be as thick as a kilometer. Matter of the inner-crust consists of electrons, free neutrons and neutron-rich atomic nuclei. As density grows the fraction of neutrons increases. The inner crust starts at the neutron drip boundary, where the neutron energy levels within the nuclei merge into a continuum and they drip outside the nuclei to comprise a free neutron gas co-existing with the crystal lattice of the neutron-rich nuclei. The neutrons in the inner crust are thought to be in a superfluid state. In this thesis we use tlie equation of state of Negele & Vautherin (1973) for the inner crust.

The density of tlie **core** is greater than 2.8 x 10^{14}gm/cc. At these densities, nuclei dissolve completely and one is left with a sea of neutrons, protons and electrons with relative abundance determined by β–equilibrium. The extent of the core goes up to the center of the star, where the densities might reach $\sim 10^{15}$ gm/cc. Most of the microscopic theories at densities of $\sim 10^{14}$ gm/cc predict the neutrons and protons to be in the superfluid and superconducting state. Laboratory experiments on properties of matter at such high densities are incomplete, and tlie reliability of the theories predicting the equation of state decreases with increasing ρ_{ns}. However, based on nucleon-nucleon scattering data from laboratory experiments various people have tried to got a handle on the equation of state at such densities. In this thesis we use the equation of state of Wiringa, Fiks & Fabrocini (1988).

1.9 Magnetic Field

Typical values of magnetic fields in pulsars as calculated using equation (1.7) lie in the range of 10^8 to 10^{13} gauss. X-ray cyclotron lines detected in accreting neutron stars also suggest fields of the order of 10^{12} gauss (e.g. Trumper et al. 1977, Wheaton et al. 1979, White et al. 1983). Though the magnetic field is of such a high value it does not alter the structure of neutron stars, as the energy scales of the ultra-dense matter are significantly high compared to the magnetic energy. However, till date there is no clear understanding regarding the origin of the magnetic field. There are primarily two schools of thought regarding the origin. One school believes that the magnetic field is the fossil field of the progenitor star and the other believes that the field is generated after the neutron star is born.

In the fossil field scenario, which was originally suggested by Woltjer (1964) even before the discovery of pulsars, the magnetic field is amplified during the collapse phase of the star. The magnetic flux, initially present in the core of the progenitor star of radius R_s, is enhanced when the star collapses to form a neutron star of much smaller radius R, without expelling the magnetic flux. Conservation of flux demands that the magnetic field of the neutron star be enhanced by a factor $(R_s/R)^2$, which is of the order of 10^{10} where $R_s \sim 10^{11}$cm for a massive star and $R \sim 10^6$ cm. To explain the observed values of 10^{12} gauss, the magnetic field of the progenitor star has to be $\sim 10^2$ gauss. Such high values of magnetic fields are however not commonly observed in massive stars, thus weakening the fossil field hypothesis. To overcome this problem, it was suggested by Ruderman & Sutherland (1973) that the field might not be a remnant of the progenitor stage but is built up during the convective carbon-burning phase just before the collapse occurs. It is however unclear whether the field that builds up in the short time scale of the carbon-burning phase followed by the collapse, is enough to give rise to the large scale poloidal fields.

The other scenario, originally proposed by Blanford et. al. (1983), suggests that the magnetic field in neutron stars can be generated due to a 'thermomagnetic' instability in the crust of the neutron star. The mechanism transforms some fraction of energy carried by the thermal flux through the medium into the energv of magnetic fields. For the instability to operate large temperature gradients are required which are quite possible in the outer crust of neutron stars. The density interval where the field generation could occur ranges from $10^7 - 10^{11}$ gcm^{-3}, and is confined to the outer regions of the crust. The field growth can happen in the liquid layer at the top of the crust and further be connected to the inside solid layer. A pre-existing horizontal component of the magnetic field is amplified exponentially with time at the cost of the heat flux carried by the degenerate electrons. The time scale of growth, as proposed by Blanford et al. (1983) is about $\sim 10^5$ years, however the available constraints from observations require the field generation to happen within a few hundred years after birth (Bliattacharya & Shukre, 1985, Bliattacharya 1987, Bliattacharya 1992). Urpin et al. (1986) showed that the thermomagnetic instability may be much more effective in the very early history of a rotating neutron star, when the layers with density $< 10^{11}$gcm^{-3} are still liquid. The field will be generated and anchored into the crust as it solidifies upon cooling.

The 'crustal model', though an attractive suggestion, has faced a number of problems. The model is only capable of generating small-scale fields in loops of the order of melting depth ~100 m. It is not clear how these small scale structures reorganise themselves within a short time to give rise to the large scale poloidal fields. Further foi the thermomagnetic instability to operate, an initial seed field of $\sim 10^8$ gauss is required whose origin is not clear.

1.10 Pulsars as probes of the Interstellar Medium

Propagation through the interstellar medium (ISM) modifies the pulsar signal in two important ways: Dispersion and Scattering.

The radio signals emitted by pulsars travel a long way through the interstellar medium before they reach the earth-bound observers. Tlie broad band radio signal thus suffers dispersion due to the ionized component of the ISM. For a homogeneous isotropic medium of ionized gas, the group velocity of propagation (v,) is a function of frequency given by,

$$v_g = c\left(1 - \frac{\nu_p^2}{\nu^2}\right)^{1/2} \approx c\left(1 - \frac{\nu_p^2}{2\nu^2}\right) \tag{1.20}$$

where ν_p is the plasma frequency which is related to the number density n_e, the mass m and charge e of the electron as $n_e e^2/\pi m$. Hence, the time taken (T) for the signal to travel a distance D from the pulsar to the observer is,

$$T = \int_0^D \frac{dl}{v_g} = \frac{D}{c} + \frac{1}{2.41 \times 10^{-4}}\nu^{-2} DM \quad \text{sec} \tag{1.21}$$

where the frequency ν is in MHz and the distance is in units of parsec (3 x 10^{18} cm). D M $= \int_0^D n_e dl$, is a measure of the total electron content between the pulsar and the observer. The second term in equation (1.21) is frequency dependent and this term gives rise to dispersive delay of the signal. Radio pulsars are observed in a frequency band $\Delta\nu = \nu_1 - \nu_2$ where ν_1 is higher than ν_2. The signal corresponding to a frequency ν_1 will arrive at a time t_1 while that at a lower frequency ν_2 will be delayed by a time At and will arrive at a time t_2, where At $= t_2 - t_1$. Thus, the pulsed signal will traverse the radio spectrum at a rate,

$$\frac{\Delta\nu}{\Delta t} = -1.205 \times 10^{-4} \frac{\nu^3}{DM} \text{MHz sec}^{-1} \tag{1.22}$$

And as a consequence the pulse will stretch out in time to a length,

$$\text{At} = 8.3 \text{ x } 10^3 \; DM\nu^{-3} \; \Delta\nu \quad \text{sec} \tag{1.23}$$

where At is also known as dispersion smearing. Thus if the pulsar is observed with very high D M and a large receiver bandwidth then the peak intensity of the pulse will reduce.

The effect of dispersion is removable and the effect is overcome by splitting the observing band into several bands with effectively smaller bandwidth called spectral channels. The pulse arrives in different spectral channels at different times, and appropriate delays using the second term in equation (1.21) is applied to align the pulses in frequency. The signal to noise ratio is effectively built up by finally adding signals from all the channels. This process is commonly known as dedispersion (Large &

Vaughan *1971)*. The DM of a pulsar can be used to find tlic distance of' the pulsar if the mean electron density ($< n_e >$) in the direction of the pulsar is known, by using $D = DM/ < n_e >$.

Pulsar signals are also affected due to the fluctuations of the electron density in the ISM. Such fluctuations gives rise to random variations in the refractive index of the medium. The pulsar signal traverses through such irregularities and gets scattered in the process. This phenomenon, known as 'Interstellar scattering' of pulsar signals and first investigated by Scheuer (1968), essentially arises due to multipath propagation of the pulsar signal. The region between the source and the observer are filled with irregularities of characteristic dimension a (refer Fig. *1.12)*. If an irregularity of dimension a has an excess electron density An, then it can be shown that the phase change $\delta\phi$ of tlic wave is $\delta\phi \approx a r_e \Delta n_e \lambda$, where λ is the wavelength and $r_e = e^2/mc^2 = 2.82 \text{ x } 10^{-13}$ cm is the classical electron radius. A ray passing a distance D encounters $\sqrt{D/a}$ irregularities. The resulting rms pliase deviation $\Delta\phi$ in ϕ becomes,

$$\Delta\phi \approx \left(\frac{D}{a}\right)^{1/2} \delta\phi = (Da)^{1/2} r_e \Delta n_e \lambda \tag{1.24}$$

This change in phase by amount $\Delta\phi$ over a transverse distance a causes the wavefront to bend by an angle θ_{sc} (where θ_{sc} is tlic scattering angle as shown in figure *1.12* panel *2)* given by, $\Delta\phi = 2\pi a \theta_{\text{sc}}/\lambda$. Using this value of $\Delta\phi$ in equation *(1.24).* we get

$$\theta_{\text{sc}} \approx \frac{\Delta\phi\lambda}{2\pi a} = \frac{1}{2\pi}\left(\frac{D}{a}\right)^{1/2} r_e \Delta n_e \lambda^2 \tag{1.25}$$

For a gaussian distribution of irregularities, the scattering angle has a gaussian angular probability distribution given by,

$$P(\theta)d\theta \propto e^{-\theta^2/\theta_o^2} d\theta \tag{1.26}$$

where θ_o is the observed half-angular width of the scattering disc such that $\theta_o = \theta_{\text{sc}}/2$ (see Fig. *1.12* panel 2), where the entire scattering process has been appoximated to be taking place in a thin screen located midway between the source and the observer (panel 2 of Fig. *1.12)*. Radiation arriving at an observer which is scattered by an angle θ to the direct path is thus delayed by an amount $\Delta t(\theta) = D\theta^2/2c$. The probability of a ray getting deviated between θ and $\theta + d\theta$, reaching tlie observer is proportional to $\theta d\theta$, which is the solid angle subtended by an annulus of radius θ and width dB. The intensity of the scattered signal is thus given by,

$$I(\theta)d\theta \approx 2\pi\theta \; e^{-\theta^2/\theta_\circ^2} \frac{d\theta}{\pi\theta_\circ^2} \tag{1.27}$$

Hence, the intensity in terms of the delay time At is given by,

$$I(\Delta t) = I(\theta)\frac{d\theta}{d\Delta t} \approx \frac{1}{\tau_{scat}} e^{-\Delta t/\tau_{scat}} \tag{1.28}$$

where $\tau_{scat} = \frac{D}{2c}\theta_\circ^2 \approx \frac{1}{2ac} \cdot \left(\frac{1}{2\pi}\right)^2 r_e^2 \Delta n_e^2 D^2 \lambda^4$.

Thus, a narrow pulse will have a sharp rise and will broaden giving rise to an exponential decay in a time scale τ_{scat} (refer Fig.1.12). The time scale τ_{scat}, known as the.scatter broadening time, is proportion l to X^4. The pulse broadening and the frequency dependence is readily observed in pulsars. If it is assumed that the electrons that are responsible for dispersion of pulsar signals are the same ones that gives rise to scattering, then we can assume a simple law that, An, $\propto$ n,. In such a case, it follows that $\tau_{scat} \propto DM^2X^4$. Observationally, τ_{scat} and DM are seen to be correlated. We tliscuss this correlation in chapter 5.

In reality, the irregularities are not of one cliaracteristic size a, but have a size distribution closer to a power law. Such a distribution can be written in the wave number space $q = 2\pi/a$, as

$$P(q) = C_n^2 q^{-\beta} \tag{1.29}$$

where β is the spectral index. Taking this distribution into account,: $\theta_\circ$ is found to scale with frequency as (Rumsey 1975, Lee & Jokippi 1975),

$$\theta_\circ \propto \lambda^{\beta/(\beta-2)} \tag{1.30}$$

and hence,

$$\tau_{scat} \propto \lambda^{2\beta/(\beta-2)} \tag{1.31}$$

For a Kolmogorov spectrum, $\beta = 11/3$, giving $\tau_{scat} \propto \lambda^{4.4}$. Scattering changes the apparent size of the source, such that the central part is broadened and a halo is produced around it. Tlic sharp leading edge comes from the central part, while the exponential

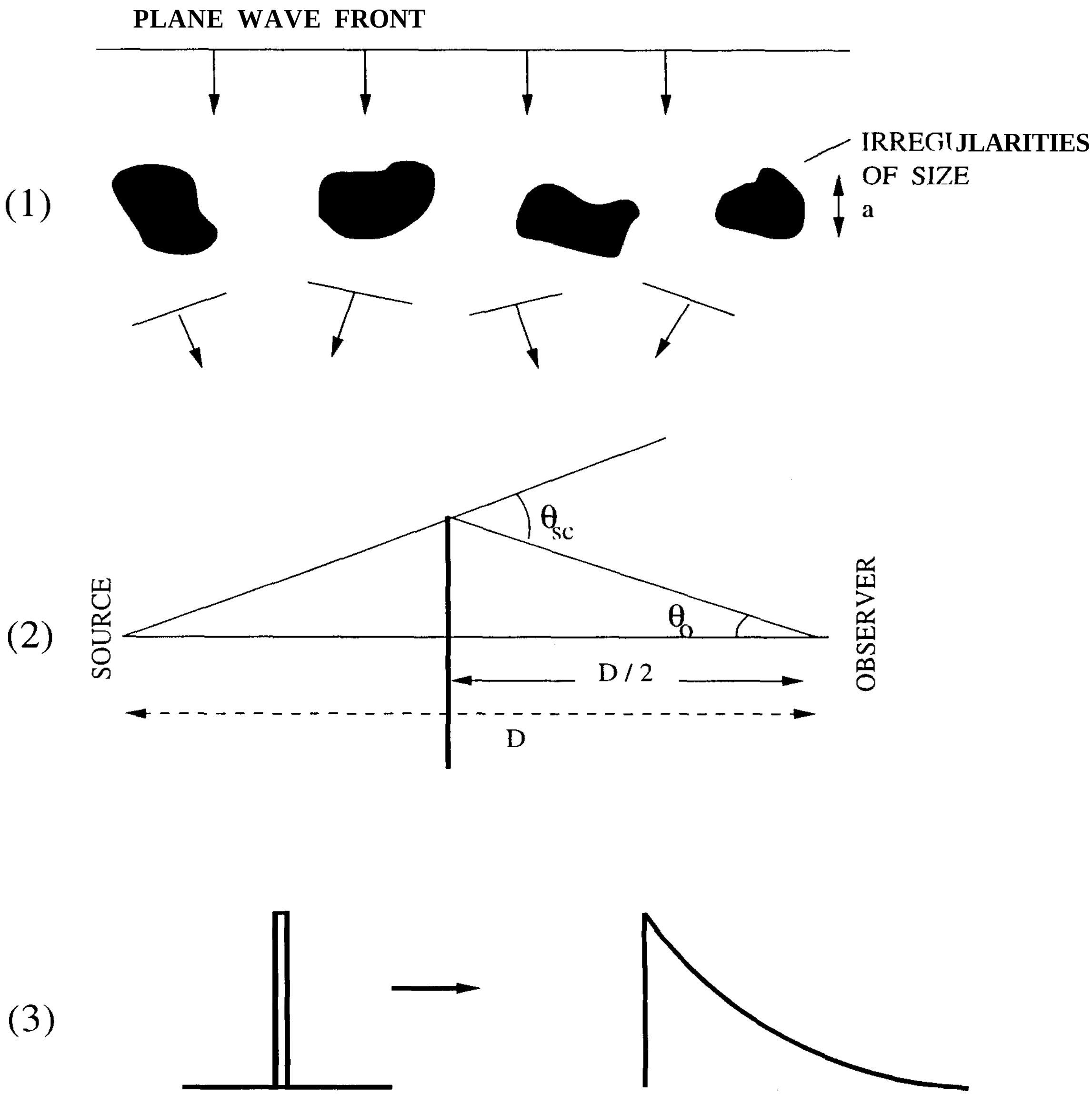

Figure 1.12: Schematic diagram illustrating the scattering of pulsar signals due to inhomogeneity in the Interstellar medium. In panel 1, the bending of the plane wave normals scattered due to inhomogeneities of size a is shown. In panel 2. the geometry of the thin screen model is shown, where the screen is approximated to be situated half way between the source and the observer. Panel 3 shows the effect of scattering on a narrow delta function which acquires an exponential tail after getting scattered.

tail comes from the halo, and thus the apparent size of the source changes during the pulse. Signals arriving from a delayed path travels an extra path $c\tau_{scat}$. The relative phases of the various signal components will range over $(2\pi/\lambda)c\tau_{scat} = 2\pi\nu\tau_{scat}$. Interference of signals with this phase range will produce a scintle pattern in the observing plane. For any relative motion between the source and the observer, amplitude variation of the intensity pattern can be observed. This is known as Diffractive Interstellar scintillation. The phase range also depends on frequency. Thus, within a given band of observation, the intensity pattern with frequency will have variations. The intensity pattern remains correlated in a frequency range till the time the phase range becomes large compared to 1 radian, beyond which the pattern is essentially decorrelated. This frequency range over which correlation exists is known as the decorrelation bandwidth. The above condition gives a very important relation between the decorrelation bandwidth, ν_s and the pulse broadening τ_{scat} as,

$$2\pi\nu_s\tau_{scat} = 1 \tag{1.32}$$

This relation (refer Lang 1971, Sutton 1977) has been proven experimentally for many pulsars. Note that at high frequencies it is difficult to measure τ_{scat} as it is extremely small to be resolved. In such cases the decorrelation bandwidth can be comfortably measured because of its inverse relationship with τ_{scat} as shown in equation (1.32).

Apart from the short term variability, pulsars are known to show intensity variations over much longer time scales. Such variations occur over time scales of many months to years. These variations are understood to be due to the large scale inhomogeneities in the interstellar medium. The slow variations are known as refractive scintillation. For an excellent review on this subject see Rickett (1977) and references therein.